

Supplementary Figures

Repeat associated mechanisms of genome evolution and function revealed by *the Mus caroli* and *Mus pahari* genomes

David Thybert^{1,2}, Maša Roller¹, Fábio C.P. Navarro³, Ian Fiddes⁴, Ian Streeter¹, Christine Feig⁵, David Martin-Galvez¹, Mikhail Kolmogorov⁶, Václav Janoušek⁷, Wasiu Akanni¹, Bronwen Aken¹, Sarah Aldridge^{5,8}, Varshith Chakrapani¹, William Chow⁸, Laura Clarke¹, Carla Cummins¹, Anthony Doran⁸, Matthew Dunn⁸, Leo Goodstadt⁹, Kerstin Howe³, Matthew Howell¹, Ambre-Aurore Josselin¹, Robert C. Karn¹⁰, Christina M. Laukaitis¹⁰, Lilue Jingtao⁸, Fergal Martin¹, Matthieu Muffato¹, Michael A. Quail⁸, Cristina Sisu³, Mario Stanke¹¹, Klara Stefflova⁵, Cock Van Oosterhout¹², Frederic Veyrunes¹³, Ben Ward², Fengtang Yang⁸, Golbahar Yazdanifar¹⁰, Amonida Zadissa¹, David Adams⁸, Alvis Brazma¹, Mark Gerstein³, Benedict Paten⁴, Son Pham¹⁴, Thomas Keane^{1,8}, Duncan T Odom^{5,8*}, Paul Flicek^{1,8*}

¹ European Molecular Biology Laboratory, European Bioinformatics Institute, Wellcome Genome Campus, Hinxton, Cambridge, CB10 1SD, United Kingdom

² Earlham Institute, Norwich research Park, Norwich, NR4 7UH, United Kingdom

³ Yale University Medical School, Computational Biology and Bioinformatics Program, New Haven, Connecticut 06520, USA

⁴ Department of Biomolecular Engineering, University of California, Santa Cruz, California 95064, USA

⁵ University of Cambridge, Cancer Research UK Cambridge Institute, Robinson Way, Cambridge CB2 0RE, UK

⁶ Department of Computer Science and Engineering, University of California, San Diego, La Jolla, CA 92092

⁷ Department of Zoology, Faculty of Science, Charles University in Prague, Prague, Czech Republic Institute of Vertebrate Biology, ASCR, Brno, Czech Republic

⁸ Wellcome Trust Sanger Institute, Wellcome Trust Genome Campus, Hinxton, Cambridge, CB10 1SA, United Kingdom

⁹ Wellcome Trust Centre for Human Genetics, Oxford, UK.

¹⁰ Department of Medicine, College of Medicine, University of Arizona.

¹¹ Institute of Mathematics and Computer Science, University of Greifswald, Greifswald, 17487, Germany

¹² School of Environmental Sciences, University of East Anglia, Norwich Research Park, Norwich, United Kingdom

¹³ Institut des Sciences de l'Evolution de Montpellier, Université Montpellier / CNRS, 34095 Montpellier, France

¹⁴ Bioturing Inc, San Diego, California

Corresponding authors: DTO (duncan.odom@cruk.cam.ac.uk); PF (flicek@ebi.ac.uk)

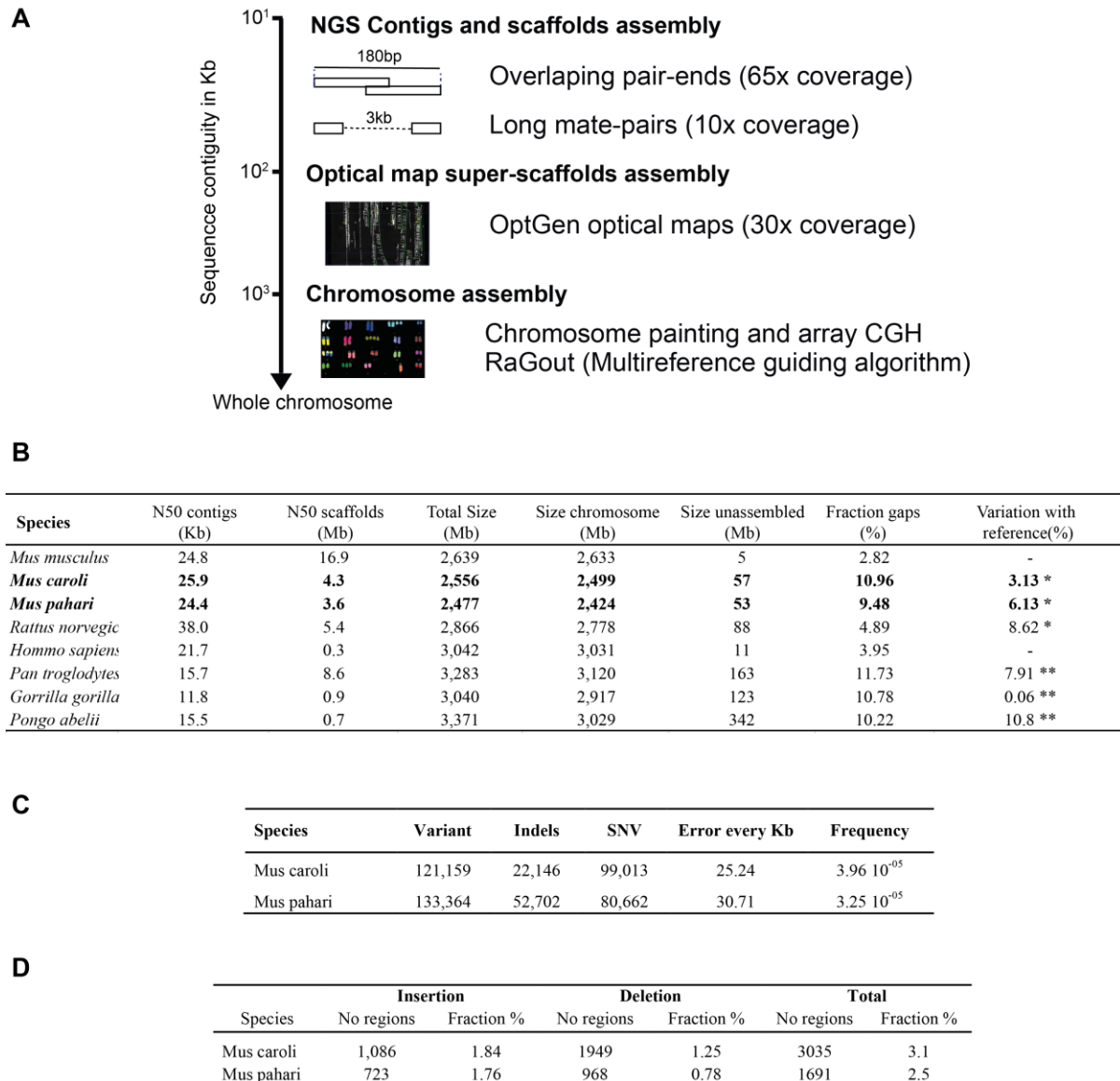


Figure S1.1. Genome sequencing and assembly strategy to create an optimal assembly of chromosomes at different contiguity level.

A. Description of the strategy for sequencing and assembly of the *Mus caroli* and *Mus pahari* genomes

B. Assembly statistics of the four Muridae and Hominidae genomes. The genomes assembled in this study are in bold. The N50 statistics for the genome not assembled in this study come from their initial genome paper.

C. Nucleotide error rates estimated by calling single nucleotide variants from mate-pair libraries mapped to the corresponding final assembly (**Method SM1.14**).

D. Estimated assembly error rates from identified inconsistencies between the corresponding optical maps aligned to the final assembly. Insertion is defined as a fragment present in the final assembly and not found in the optical map data. Deletion is defined as a fragment found in the optical map data and not in the final assembly.

A

Species	Protein coding	Non coding RNA	To be experimentally confirmed	Total
<i>Mus musculus</i>	22,501	12,923	2,264	37,688
<i>Mus caroli</i>	20,323	10,069	1,978	32,370
<i>Mus pahari</i>	20,029	9,336	1,847	31,212
<i>Rattus norvegicus</i>	22,277	8,825	25	31,127
Human	20,246	24,690	1,053	45,989
Chimpanzee	18,759	8,681	0	27,440
Gorilla	20,962	6,701	0	27,663
Orangutan	20,424	6,996	0	27,420

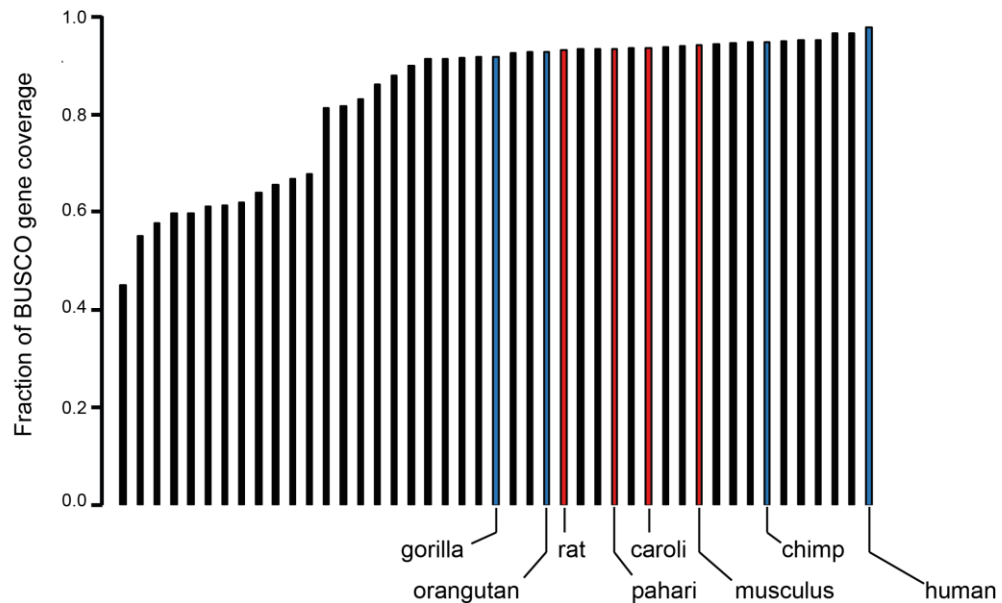
B

Figure S1.2. *Mus caroli* and *Mus pahari* shows similar annotation statistics and gene completeness than the primates genome sequenced with equivalent technology.

A. Annotation statistics for the four Muridae and Hominidae genomes. *Mus caroli* and *Mus pahari* have been annotated by integrating three different annotation pipelines and RNA-seq data (**Method SM1.5**). The annotation of the other genomes is from Ensembl v83.

B. Gene completeness as measured by the BUSCO dataset for all mammalian genomes available in Ensembl v83 (only the four Muridae (red) and four Hominidae (blue) are labeled). The plot represents the median of the fraction aligned for those members of the BUSCO gene set that align to the genome. The Muridae and Hominidae genomes have similar completeness.

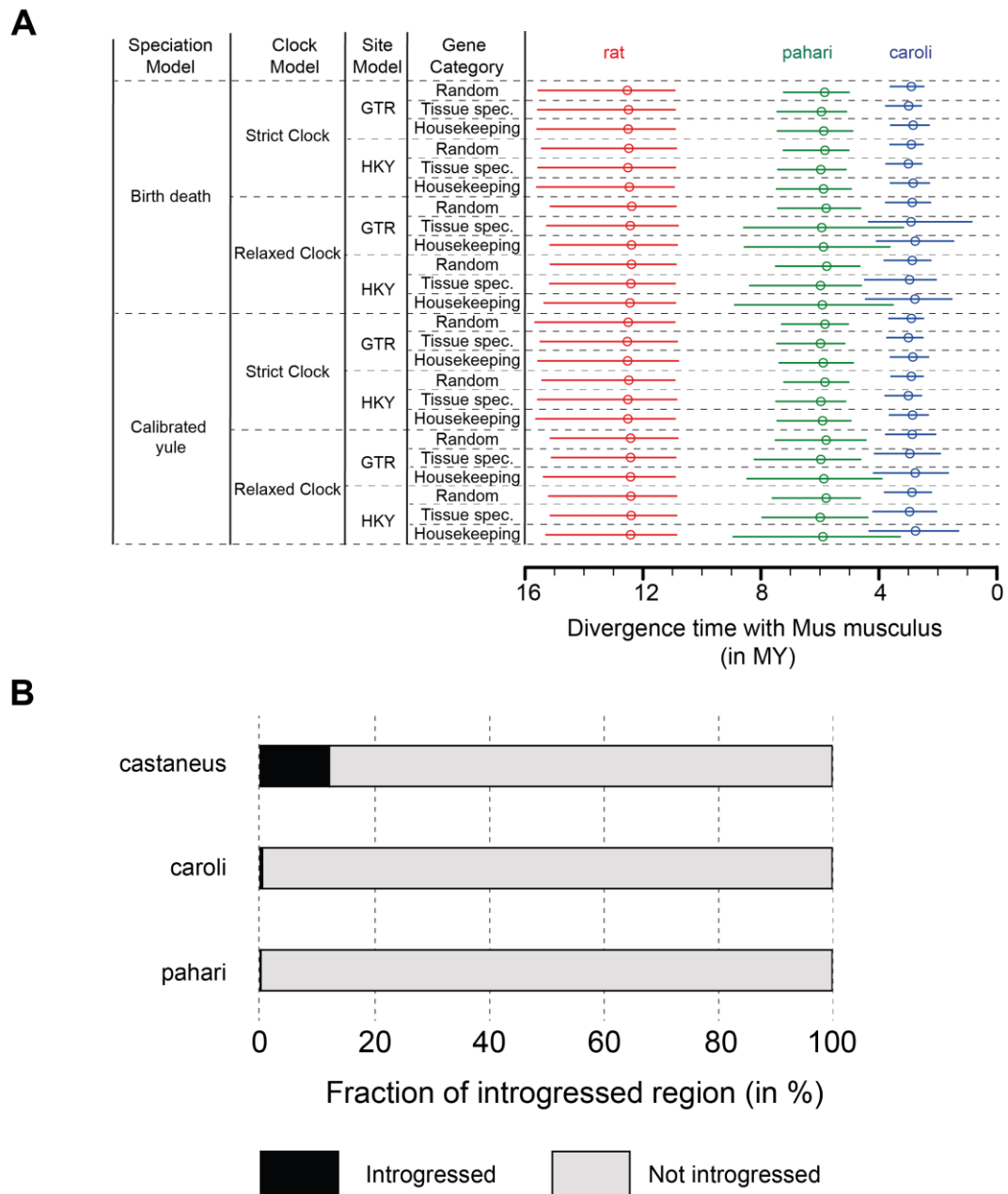


Figure S1.3. Divergence time estimation for *Mus musculus*, *Mus caroli* and *Mus pahari* is robust to the model used.

A. Estimation of *Mus caroli*, *Mus pahari* and Rat divergence time using different evolutionary models and different sets of coding genes.

B. Fraction of the genome introgressed with *Mus musculus*. *Mus castaneus* is used as positive control.

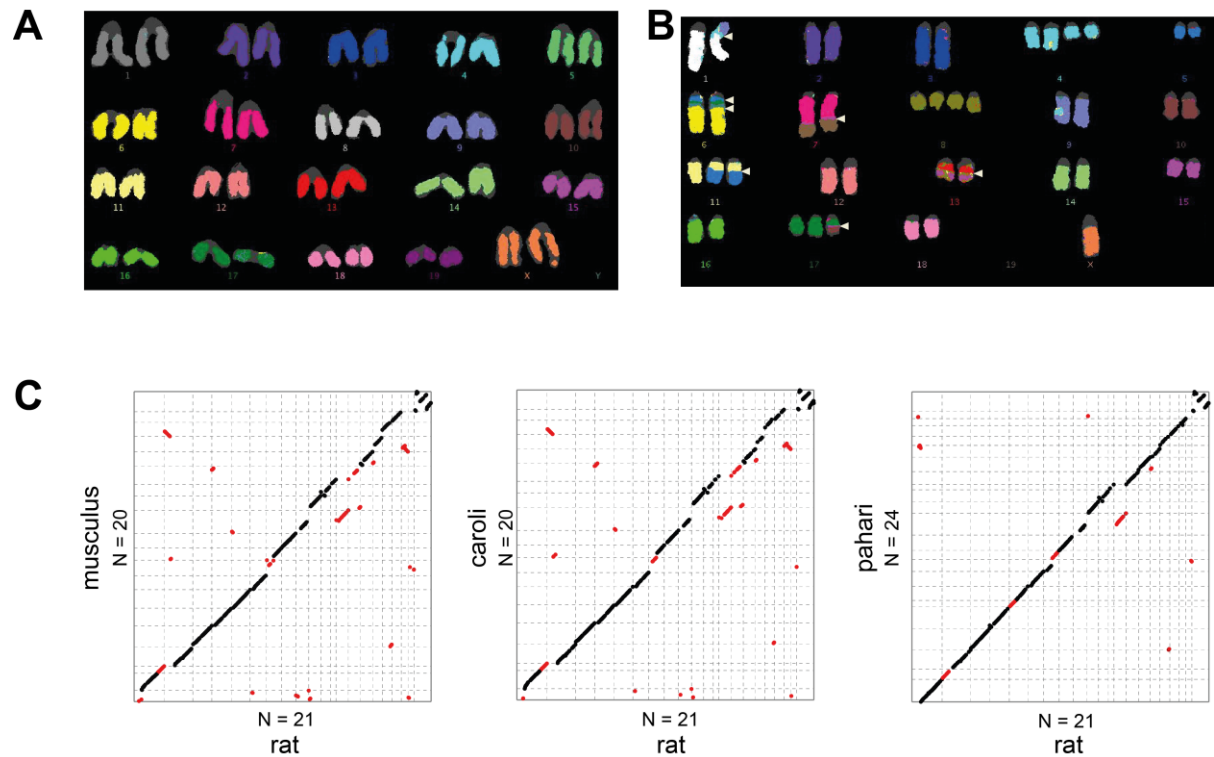


Figure S1.4. The ancestor of *Mus musculus* and *Mus caroli* underwent a largescale rearrangement as compared with *Mus pahari*.

A. DNA FISH of *Mus caroli* karyotype using *Mus musculus* probs.

B. DNA FISH of *Mus pahari* karyotype using *Mus musculus* probes. White arrows identify the break points of major rearrangements.

C. Dot plot showing pairwise comparison of the rat chromosomes with the three *Mus* species. The inter-chromosomal rearrangements are shown in red.

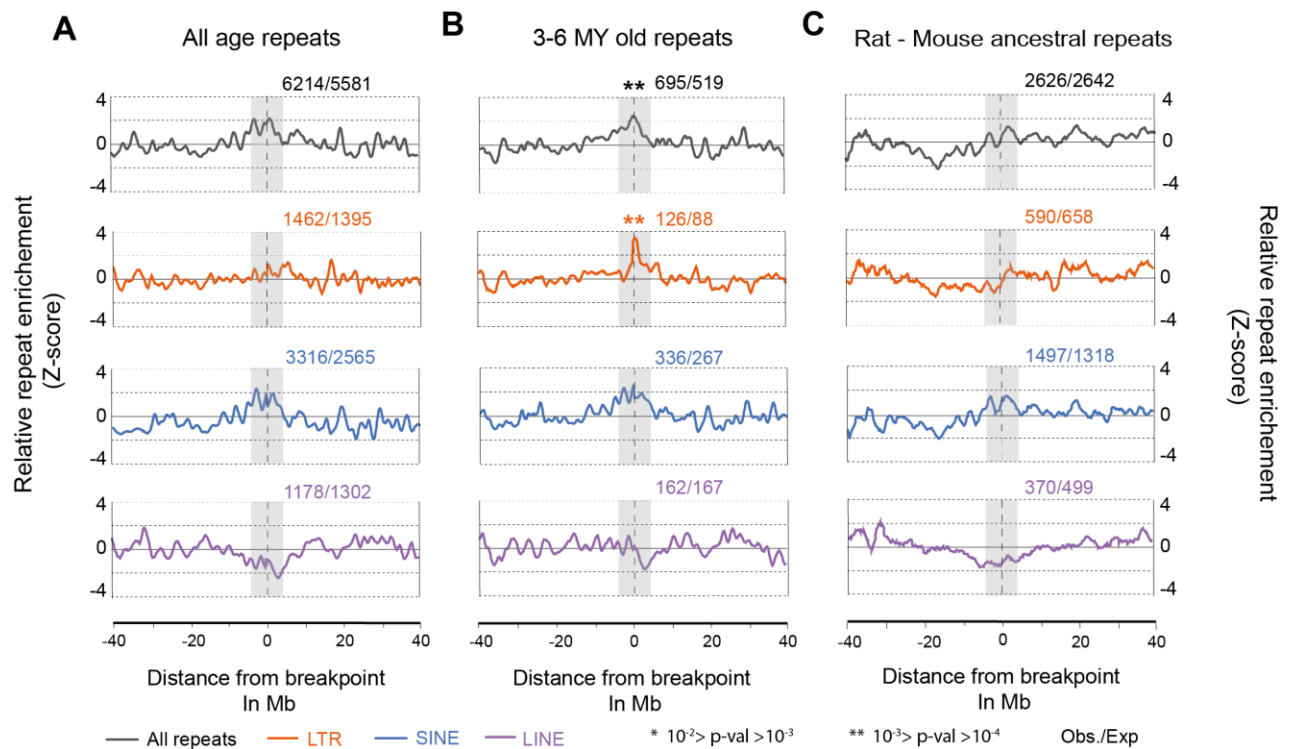


Figure S1.5. The inter-chromosomal break points between *Mus musculus* and *Mus pahari* are enriched with 3-6MY old LTR retrotransposons.

A Density of all retrotransposons regardless of age plotted by distance to break points of inter-chromosomal rearrangements larger than 3MB. No significant enrichment was observed.

B Density of 3-6MY old retrotransposons plotted by distance to break points of inter-chromosomal rearrangements larger than 3MB. These retrotransposons appeared concurrent to the punctate event of chromosomal rearrangement. LTRs are significantly enriched at these break points.

C Density of the mouse-rat ancestral repeats by distance to break points of inter-chromosomal rearrangements larger than 3MB. No significant enrichment was observed.

For A-C, the ratio on the top of each plot show the number of observed element relative to the expected (**Method SM 2.3**).

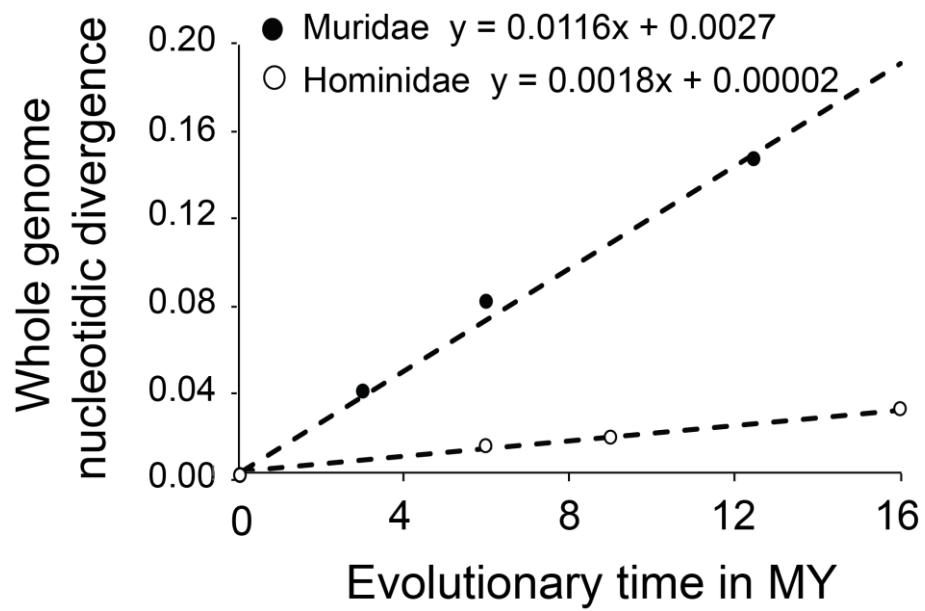


Figure S2. Acceleration of Whole genome nucleotide mutational rates in the Muridae lineage. Nucleotide evolutionary rate calculated from whole genome in Muridae (black) and in Hominidae (white).

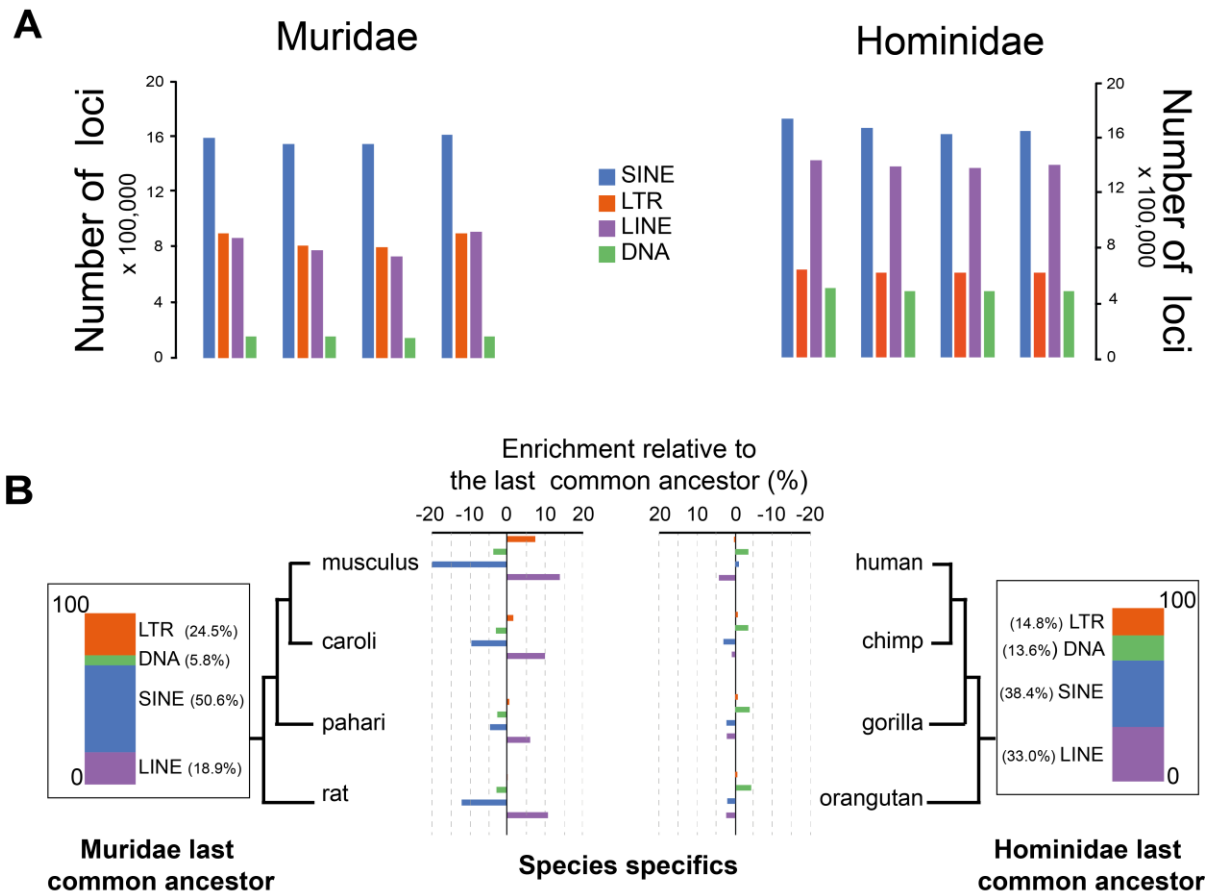
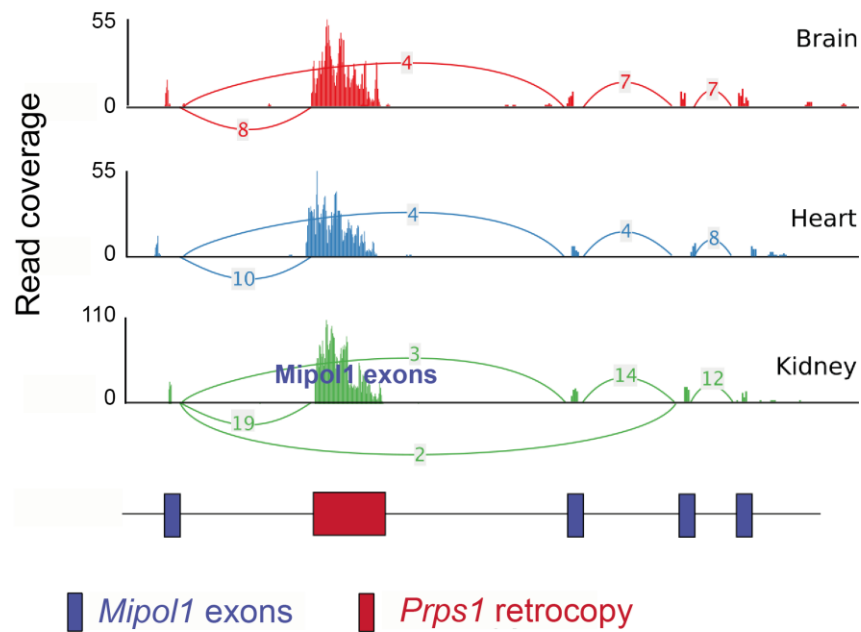


Figure S3.1. Transposable elements have different activity history between the two lineages.

A Breakdown of the number of transposable elements for each class in the species of the two lineages. The numbers of transposable elements from the four major classes are highly stable intra-lineage and vary between lineages. LINE elements tend to be shorter in Hominidae compared to Muridae (average 382 bp vs 563 bp) meaning that even though the number of loci differ between the clades, the genome coverage is approximately the same (e.g. mouse 19.1%; human 18.7%).

B Species-specific transposable elements are enriched in LINEs in Muridae. The enrichment has been calculated with regard to a set of ancestral transposable elements. Statistical significance uses a Fisher test.

A**B**

Chimeric Transcript

Mipol1 *Prps1*
 CTTGCCTCCGCCGCCGACA CTGAGGAGCCGCGGGATCC

Figure S3.2. Example of a genomic locus carrying a chimeric gene that involves the host gene *Mipol1* and a *Prps1* retrocopy.

A Gene expression profile of the different exons of the chimeric gene in the brain, heart and kidney. The colored arcs represent links between exons in the spliced transcripts. The label on each arc represents the number of reads supporting the association between exons in the final spliced transcript.

B Nucleotide sequence of the chimeric transcript around the *Mipol1*-*Prps1* junction

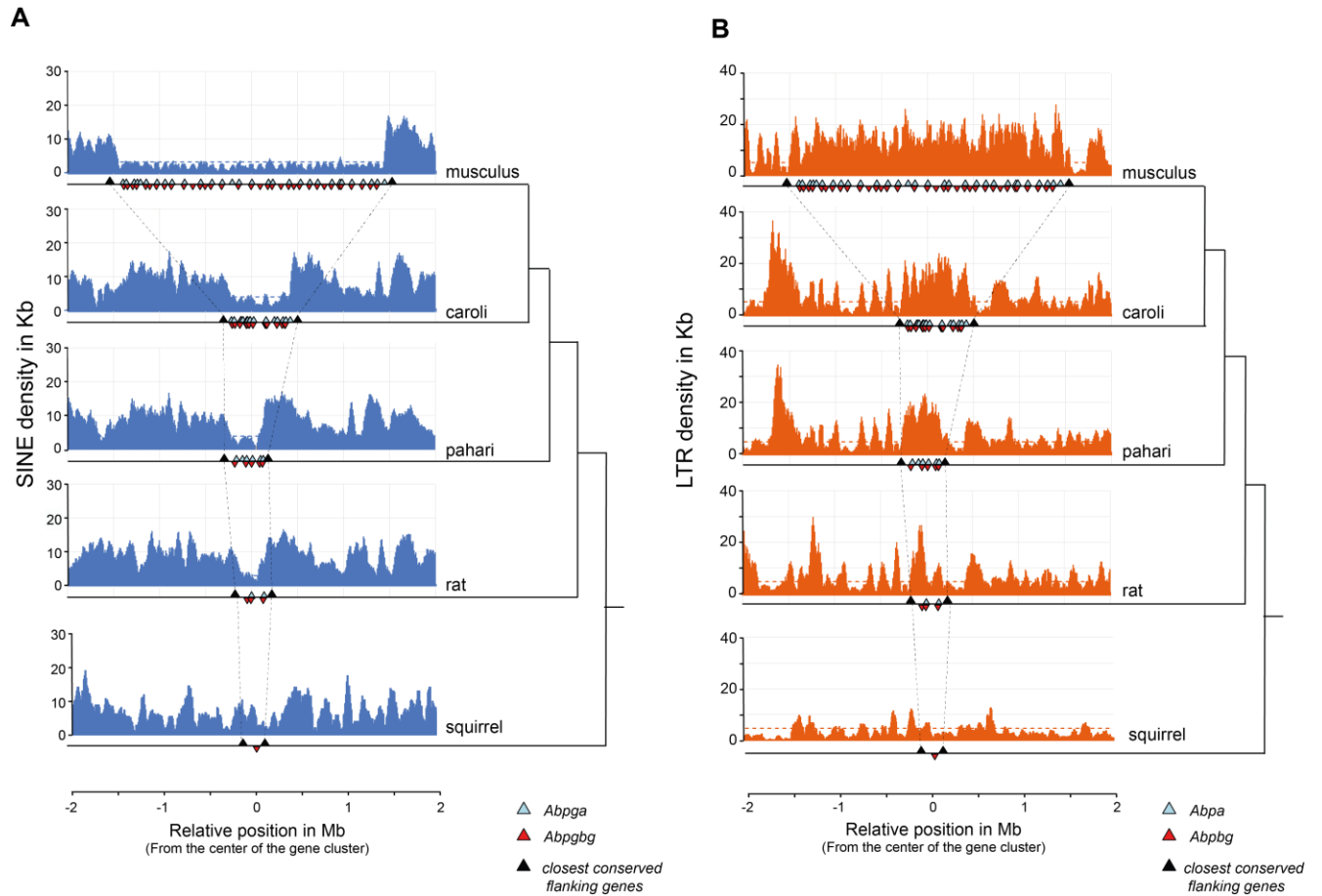


Figure S3.3. LTR retrotransposons are enriched in the *Shbg* gene cluster while SINEs are depleted.

A Density of SINE elements in the *Abp* gene cluster of the *Mus musculus*, *Mus caroli*, *Mus pahari*, the rat genomes and the squirrel. The blue and red triangles represent the *Abp* genes (*Abpa* in blue, *Abpbgb* in red); black triangles represent the closest flanking genes (upstream: *Scn1b* and downstream : *Gpi1*) shared by the four Muridae species.

B Density of LTR elements in the *Abp* gene cluster of the *Mus musculus*, *Mus caroli*, *Mus pahari*, the rat genomes and the squirrel. The blue and red triangles represent the *Abp* genes (*Abpa* in blue, *Abpbgb* in red); the black triangles represent the closest flanking genes (upstream: *Scn1b* and downstream : *Gpi1*) shared by the four Muridae species.

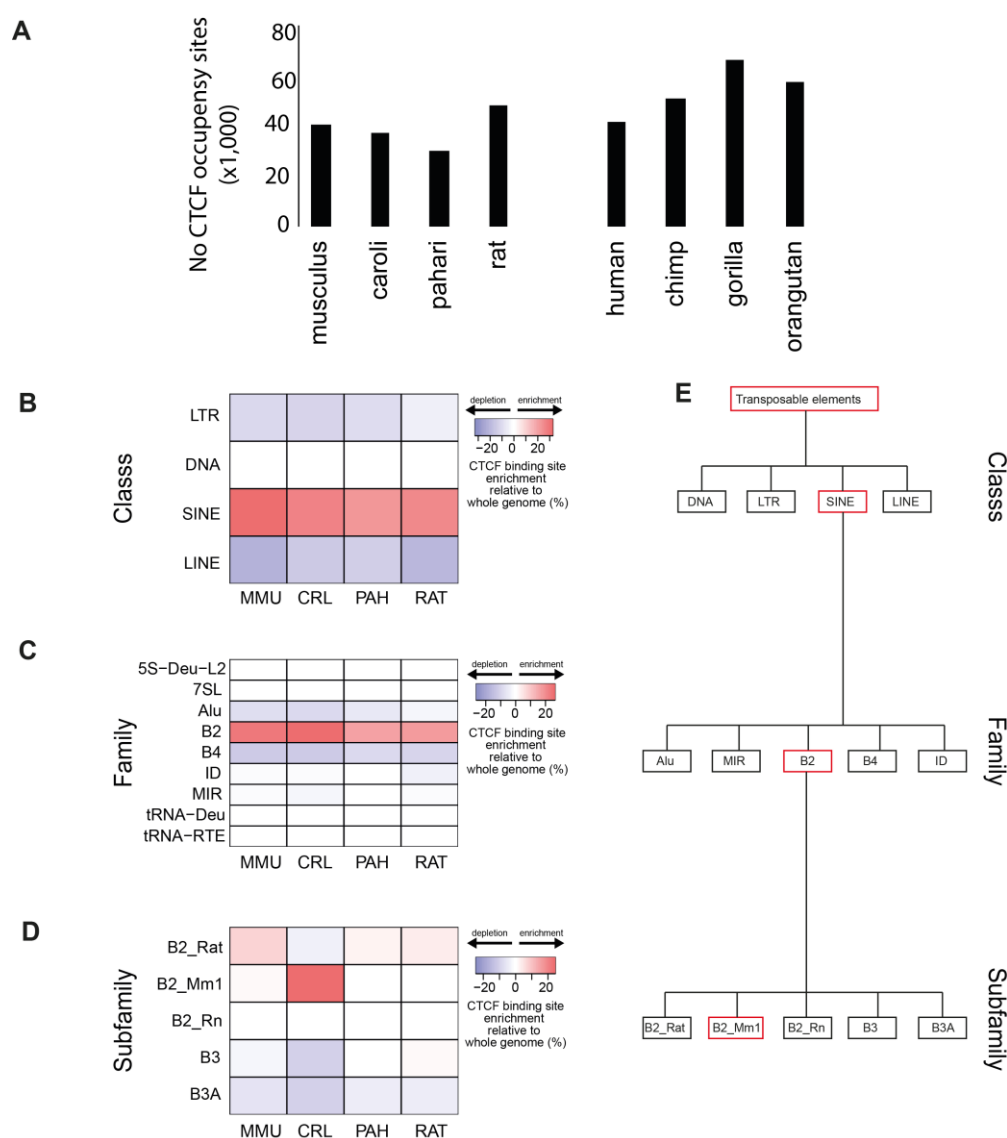


Figure S4.1. Mus caroli show a species-specific enrichment of SINE B2_Mm1 elements carrying CTCF binding.

A Breakdown of the number CTCF binding sites identified in the Muridae and Hominidae species

B Overrepresentation of the class of the transposable elements carrying CTCF binding sites

C Overrepresentation of the family of the SINE elements carrying CTCF binding sites

D Overrepresentation of the sub-family of the B2 elements carrying CTCF binding sites.

In B-D MMU= *Mus musculus*; CRL= *Mus caroli*; PAH= *Mus pahari*; RAT= Rat

E Classification hierarchies of the SINE B2 subfamilies. The red boxes show the classification hierarchy of the B2_mm1 elements.

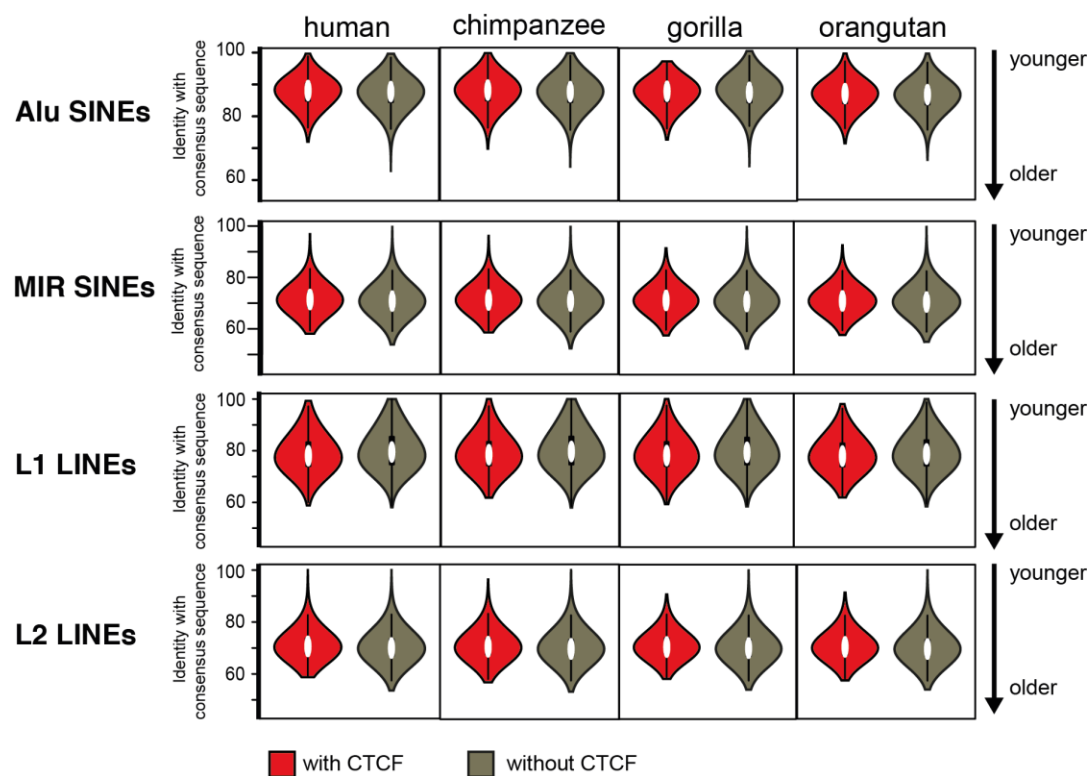


Figure S4.2. Identity plot of each transposable element with its subfamily consensus in the four Hominidae species. Elements carrying CTCF are in red and those not carrying CTCF are in brown.

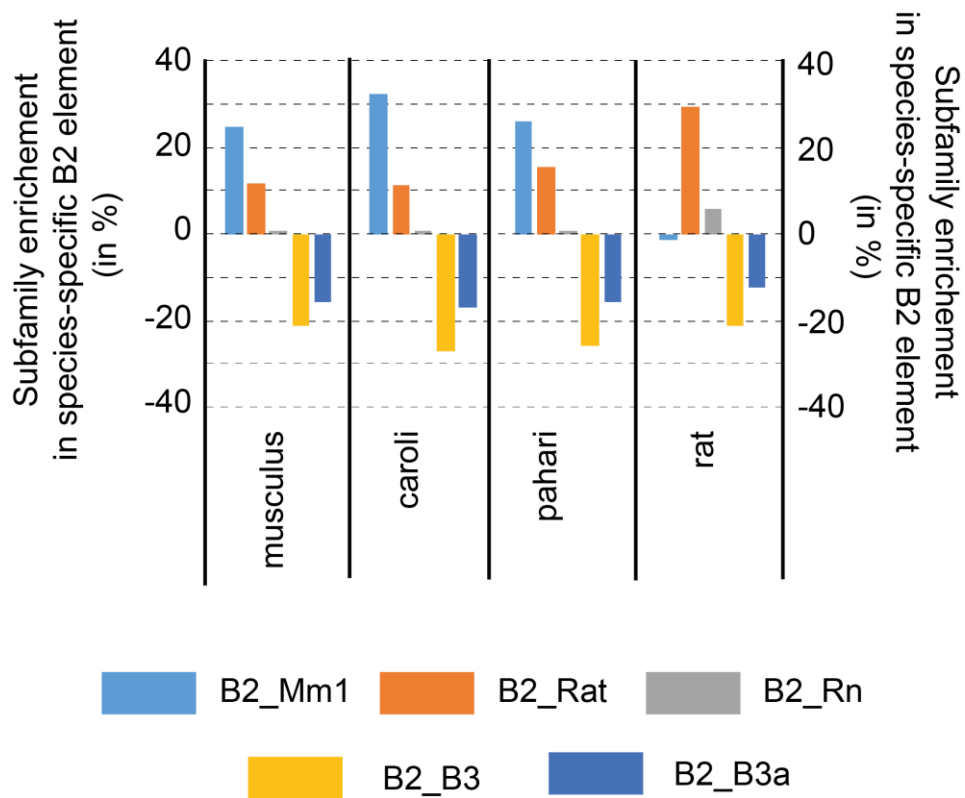


Figure S4.3. The species-specific SINE B2_Mm1 repeats are enriched in the three *Mus* species. SINE B2_Mm1 repeats have a species-specific enrichment limited to the three *Mus* species when compared to a set of ancestral transposable elements.

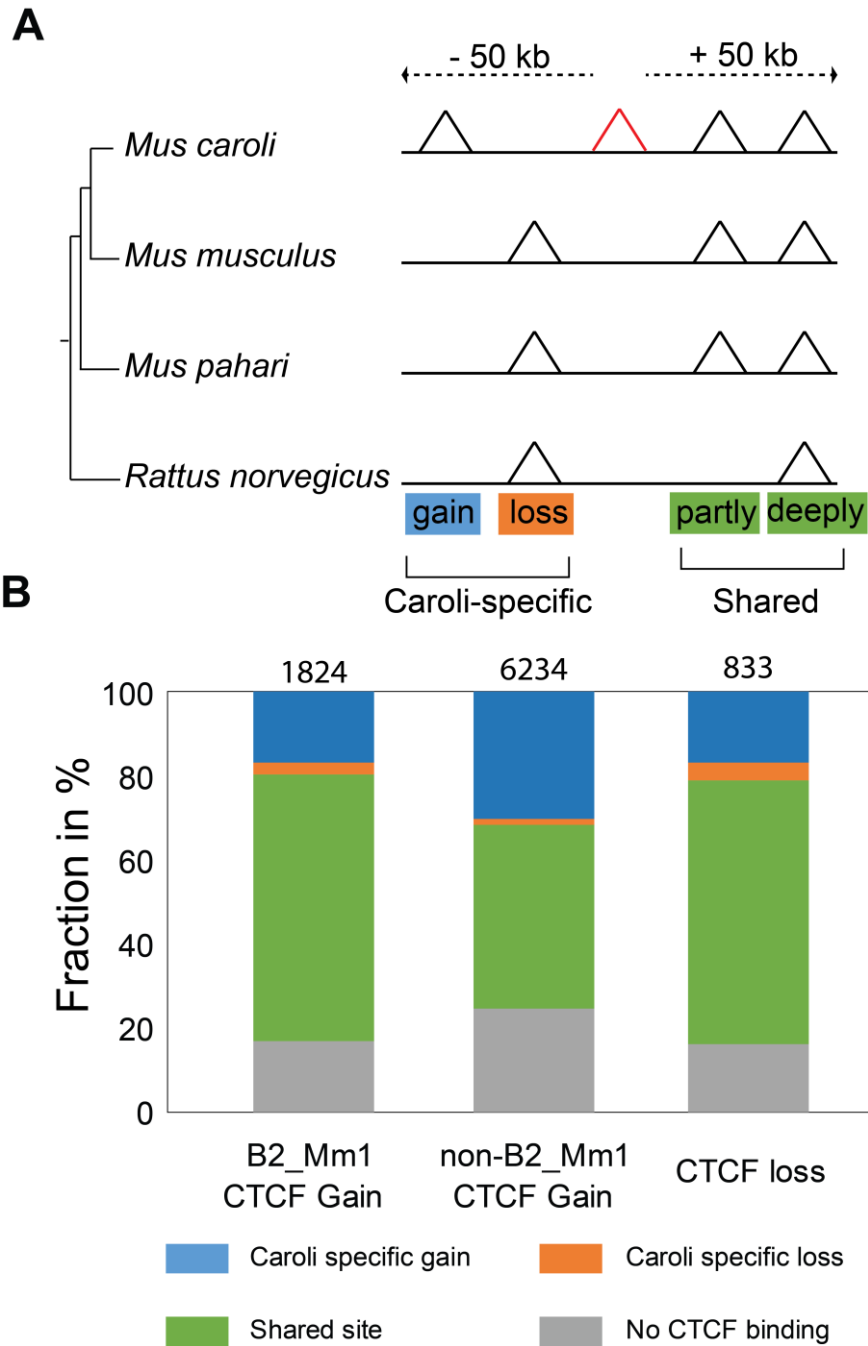


Figure S4.5. B2_Mm1 expanded CTCTF binding occurs in CTCTF rich regions.

A *Mus caroli* specific CTCTF binding gains or losses (red central peak) are classified by whether they occurred close to (i) CTCTF binding gains specific to *Mus caroli* (ii) CTCTF binding losses specific to *Mus caroli*, or (iii) CTCTF binding shared between *Mus caroli* and the other Muridae.

B Fraction of *Mus caroli* CTCTF binding gains associated with the monophyletic B2_Mm1 repeat (left column) that are close to (i) *Mus caroli* specific CTCTF binding gains (blue), (ii) *Mus caroli* specific CTCTF binding losses (orange) (iii) *Mus caroli* CTCTF binding shared with other Muridae (green) or no CTCTF binding (grey). Middle column displays fractions not associated with a B2_Mm1 repeat and right column fractions associated with *Mus caroli* specific CTCTF binding losses